Measurements and numerical simulation of fabric evolution along the Talos Dome ice core, Antarctica

M. Montagnat, D. Buiron, L. Arnaud, A. Broquet, P. Schlitz, R. Jacob, S. Kipfstuhl

Measurements and numerical simulation of fabric evolution along the Talos Dome ice core, Antarctica

M. Montagnat[a,], D. Buiron[a], L. Arnaud[a], A. Broquet[a], P. Schlitz[a], R. Jacob[a], S. Kipfstuhl[b]

[a] *LGGE UMR5183, CNRS / UJF - Grenoble 1, Saint-Martin d'Hères, France*
[b] *Alfred Wegener Institute for Polar and Marine Research, Columbusstrasse, D-27568 Bremerhaven*

Abstract

We present measurements of fabrics and microstructures made along the Talos Dome ice core, a core drilled in East Antarctica in the framework of the TALDICE project. Fabric and average grain size data are analyzed regarding changes in climatic conditions. In particular, the fabric strength increases sharply going downward from Holocene to Wisconsin ice. Following (Durand et al., 2007), this change is associated with a positive feedback between variations in ice viscosity, due to variations in dust content, and the impact of a shear stress component, increasing with depth. A ViscoPlastic Self Consistent modeling approach is used to simulate the fabric evolution for a "perfect dome" configuration. The discrepancies between the measured and the simulated fabrics highlight the depth ranges where shear strongly affects the fabric strengthening. Finally, the grain size and fabric analyses show the occurrence of dynamic recrystallization mechanisms (continuous

Email address: maurine.montagnat@univ-grenoble-alpes.fr (M. Montagnat)
URL: http://www-lgge.obs.ujf-grenoble.fr/~maurine/maurine.html (M. Montagnat)

and discontinuous) along the core.

This version is the personal copy of the article published in EPSL:

http://dx.doi.org/10.1016/j.epsl.2012.09.025

Keywords: ice core, fabric, grain size, VPSC model, chronology

---

1. Introduction

A 1620 m deep ice core was drilled at Talos Dome in East Antarctica in the framework of the TALDICE (TAlos Dome Ice CorE) project (www.taldice.org) during the field seasons 2004-2008. Talos Dome is a peripheral dome, located in the Ross Sea sector (Urbini et al., 2006). The TALDICE coring site (159° 11'E 72° 49'S; 2315 m a.s.l.; annual mean temperature -41°C) is located 5 to 6 km SE from the dome summit, along the main ridge (Urbini et al., 2006). The current accumulation rate is of 85 mm ice equivalent per year and is quite uniform 5 to 10 km from the summit (Stenni et al., 2002; Frezzotti et al., 2007; Urbini et al., 2008). The temperature along the coring hole was not measured. An estimation was given in the field of a bottom temperature close to -20°C. This estimate comes from the measured temperature of the bottommost core when removed from the borehole.

The entire TALDICE ice core provides a paleoclimatic record covering at least 250 kyr BP back to Marine Isotope Stage 7.5 (MIS 7.5), with the start of the last deglaciation at around 820 m depth (Buiron et al., 2011). Owing to the relatively high accumulation rate, the record benefits from a decadal scale resolution.

The coring site was chosen close but not at the geographical dome, in a

location on top of a relatively flat bedrock, in order to reduce the effect of flow perturbations on the climatic signal (Bianchi et al., 2003; Urbini et al., 2006). Very inclined tephra layers are observed below 1460 m depth. They indicate a non negligible contribution of a shear stress component on the ice flow which is coherent with the fact that the coring site is located down the ridge from the dome summit. This contribution could also be intensified by the topology of the bedrock close to the Talos Dome coring site. Indeed, the last 200 m of the core are located close to a deep valley, with abrupt elevation changes, as shown in the radargram in Fig. 1.

Ice flow is known to be strongly influenced by the induced anisotropy that develops during deformation in ice sheet conditions, in the form of preferred ice crystal orientations (see Castelnau et al. (1998); Gillet-Chaulet et al. (2006); Pettit et al. (2007) for instance). Under deformation conditions typical around ice cores, the c-axes of the ice crystals rotate towards a compression axis, perpendicular to a shear direction, and away from a tension axis (Gow and Williamson, 1976; Alley, 1988; Paterson, 1994). The c-axis distribution (referred to as fabric in the following) along a core is then a good candidate to evaluate the nature of the flow and to extract some irregularities in the deformation history.

In the specific case of a perfect dome, the ice deforms mainly by compression along the vertical direction (Alley, 1988). This is qualitatively confirmed by the fabrics measured along cores such as the ones of GRIP (Thorsteinsson et al., 1997), Dome Fuji (Azuma et al., 1999), or EPICA Dome C (Wang et al., 2003; Durand et al., 2009) which are all located at geographical domes. Nevertheless, deviations from the "perfect dome" tendency, and local vari-

ations of the fabric strengthening are observed along these cores. They are mostly observed at depths corresponding to climatic changes (termination 1, Holocene - Wisconsin transition, at 1500 m depth along the GRIP ice core (Thorsteinsson et al., 1997), termination 2 at 1750 m depth, along the EPICA Dome C ice core (Durand et al., 2009)). Below 2800 m depth, very similar abrupt variations in the fabric signal were measured along the GRIP and EPICA Dome C ice cores. They were attributed to dynamic recrystallization mechanisms (Thorsteinsson et al., 1997; Durand et al., 2009).

Dynamic recrystallization mechanisms (DRX) are known to accommodate the deformation as observed along ice cores. The three main processes are classically described as being, successively from the top of the cores, normal grain growth, continuous (or rotation) dynamic recrystallization and discontinuous (or migration) dynamic recrystallization (de la Chapelle et al. (1998) for instance). All of them are well documented in materials science (Humphreys and Hatherly, 2004). Normal grain growth is mostly driven by the decrease in the grain boundary energy. During continuous DRX, new grains are formed by the progressive rotation of subgrains during straining, with little accompanying boundary migration. The kinetics of the grain size increase is similar to the one measured during normal grain growth (de la Chapelle et al., 1998; Montagnat and Duval, 2000). These two mechanisms should not strongly impact the fabric, but continuous DRX could slow the c-axis strengthening under compressive strain (Castelnau et al., 1996b). The occurrence of discontinuous recrystallization is characterized by abrupt changes in grain size, shape and orientation. It is driven by a high stored deformation energy, and favored by a high value of grain boundary migra-

tion rate. These conditions are mainly encountered in the bottom part of the cores (Azuma et al., 1999; Wang et al., 2003; Durand et al., 2009).

Changes in fabrics, grain sizes and/or impurity contents can induce changes is viscosity between layers, and could induce differences in fabric evolution with depth for a similar state of stress. Along the EPICA Dome C ice core, Durand et al. (2007) calculated the impact on flow of an abrupt strengthening of the fabric similar to the one they measured at 1750m depth during termination 2. They used an anisotropic 2D ice flow model (Gillet-Chaulet et al., 2006) to quantify the impact of this change on ice flow and concluded that a positive feedback is initiated when a shear stress affects the flow. Indeed, more clustered fabrics become easier to shear, which in turn enhances the clustering (Paterson, 1991). Such observations are in favor, at least qualitatively, of a non negligible role of local changes in viscosity associated with climatic conditions, on flow heterogeneities.

At a larger scale, recent modeling efforts using finite element computation, have demonstrated the effects of anisotropy on ice flow (Gillet-Chaulet et al., 2006; Pettit et al., 2007; Seddik et al., 2008). Martín et al. (2009) showed the strong impact of the anisotropy and the non-linearity of ice rheology on the age-depth relation along a divide and Pettit et al. (2011) showed the strong influence of fabrics on the pattern of flow near the divide at Siple Dome (Antarctica).

We present here the fabric measurements performed along the Talos Dome ice core, using an Automatic Ice Texture Analyser (AITA) (Russell-Head and Wilson (2001), http://www.russellheadinstruments.com) which provides c-

axis values at a resolution of 43 μm^2 and about 5°(section 2). We use a ViscoPlastic Self Consistent (VPSC7) (Lebensohn et al., 2005) scheme under the crude assumption of compression at a constant strain rate, in order to model the fabric strengthening along the core in a perfect dome configuration (section 3). This VPSC model integrates both anisotropy and non-linearity of the ice rheology but does not reproduce dynamic recrystallization mechanisms. Section 4 provides the analyses of the measurement and modeling results, and demonstrates the benefits from combining both approaches to extract information about the flow conditions along the core.

2. Fabric and grain size measurements along the Talos Dome core

2.1. Measurements

Fabrics (c-axis orientations) were measured along the full Talos Dome core, every 10 to 20 m, from 18 m depth down to 1611 m depth. The AITA provides c-axis orientations from thin sections of dimensions up to 12 × 12 cm^2, every pixel of 43 μm^2 size. The orientation data are further represented in Schmidt pole figures. Orientation measurements are provided together with a quality factor which makes possible the elimination of pixels with too low a resolution, such as grain boundary pixels (Peternell et al., 2011).
The c-axis orientation $\mathbf{c}^k$ is defined by two angles: the co-latitude $\theta_k \in [0, \pi/2]$ (or tilt angle) and the longitude $\varphi_k \in [0, 2\pi]$ given in the local reference frame, $\boldsymbol{R}$, with the third axis perpendicular to the thin section. The expression of $\mathbf{c}^k$ in this reference frame is;

$$\mathbf{c}^k = (cos\varphi_k sin\theta_k, sin\varphi_k sin\theta_k, cos\theta_k) \quad (1)$$

Following Durand et al. (2006a) the second-order orientation tensor $\mathbf{a}^{(2)}$ was used to characterize the c-axis orientation distribution. $\mathbf{a}^{(2)}$ is defined as:

$$\mathbf{a}^{(2)} = (1/N_p) \sum_{k=1}^{N_p} \mathbf{c}^k \otimes \mathbf{c}^k \tag{2}$$

where $\mathbf{c}^k$ is given by Eq. (1), and N_p is the total number of pixels over which the $\mathbf{c}^k$ values are obtained for a given sample (thin section). Since the $\mathbf{c}^k$ values are obtained at a pixel size, the definition of $\mathbf{a}^{(2)}$ given by Eq. (2) implicitely takes into account the volume fraction of grains.

By construction, $\mathbf{a}^{(2)}$ is symmetric and there exists a symmetry reference frame, $\mathbf{R}^{sym}$ (or principal reference frame), in which $\mathbf{a}^{(2)}$ is diagonal. Let $a_i^{(2)}$ (i=1,2,3) denote the three corresponding eigenvalues and $\mathbf{e}_i$ (i=1,2,3) the associated eigenvectors (the three base vectors of $\mathbf{R}^{sym}$). The eigenvalues of $\mathbf{a}^{(2)}$ can be seen as the lengths of the axes of the ellipsoid that best fits the density distribution of grain orientations. The eigenvectors give the directions of the axes of the ellipsoid.

The three eigenvalues $a_1^{(2)}$, $a_2^{(2)}$ and $a_3^{(2)}$ follow the relations :

$$a_1^{(2)} + a_2^{(2)} + a_3^{(2)} = 1 \tag{3}$$

$$0 \leq a_3^{(2)} \leq a_2^{(2)} \leq a_1^{(2)} \leq 1 \tag{4}$$

For an isotropic fabric, $a_1^{(2)} = a_2^{(2)} = a_3^{(2)} = 1/3$, and when the fabric is transversely isotropic, two of the eigenvalues are equal:

$$\begin{aligned} &a_2^{(2)} \approx a_3^{(2)} < 1/3 \quad \text{for a single-maximum fabric,} \\ &a_1^{(2)} \approx a_2^{(2)} > 1/3 \quad \text{for a girdle fabric} \end{aligned} \tag{5}$$

Errors in the data can have several origins. In the following, we present several approaches used to estimate the various components of this error.

The first approach consisted in changing, manually, the correction criterion which makes possible the elimination of data with too low a reliability (mainly based on the quality factor data provided by the analyzer). Standard deviations smaller than 0.01 were obtained over extreme manual adjustments. The second source of error was associated with the angle range of accuracy of the analyzer measurements. A normal distribution, with a standard deviation equal to this error range was added to the measured azimuth and colatitude data. Calculations of the orientation tensor eigenvalues were then performed on a sufficient number of samplings extracted from this reconstructed data set. The obtained standard deviation, for different error angles was lower than 0.001. Finally, a bootstrap approach (Efron and Tibshirani, 1993; Palm, 2002) was used to theoretically estimate the standard deviation of the measured eigenvalues based on a re-sampling of angle data at each depth, standard deviations lower than 0.0003 were obtained. Considering the very low values of the standard deviations obtained with these three techniques, they were not taken into account in the standard deviation value. Another source of error is the one induced by a sampling on a limited number of grains. We estimated this error following Durand et al. (2006a). This method used a 3D-Pott model to evaluate the influence of the undersampling of a sample of 10 000 grains on the evaluation of the orientation tensor eigenvalues. They obtained a relation between the standard deviation, the number of grains in the thin section, N_g, and the eigenvalue, Eq. (6).

The same relation applies for the three eigenvalues.

$$\sigma(a_i) = \left[-1.64 \times (a_1^{(2)})^2 + 1.86 \times a_1^{(2)} - 0.14\right] \times N_g^{-1/2}. \quad (6)$$

Data and error bars corresponding to a $\pm 1\sigma$ confidence interval are reported in Fig. 2.

Grain sizes were measured along the core by extracting grain size contours out of the orientation-colored images provided by the AITA. Manual corrections were applied systematically. The size of a grain corresponds to the square root of the surface occupied by the grain on the binary image obtained. Standard deviation due to the sectioning effect (to obtain a grain size radius out of a 2-D section) and to the limited number of grains were evaluated following (Durand et al., 2006a) estimates. As for the standard deviation on the fabric measurements, they used the 3-D Potts model with a 3-D microstructure of a large number of grains further under-sampled (Gagliardini et al., 2004). The Potts model is known to properly reproduce the topological, grain-size distribution and morphological features of natural ice microstructures (Anderson et al., 1989). The obtained standard deviation is given by Eq. (7).

$$\sigma(< R >) \approx (0.02 + 0.44 \times N_g^{-1/2}) \times < R >, \quad (7)$$

with $< R >$ the average grain size, and N_g the number of grains in the thin section.

Fig. 5 represents the grain size evolution with error bars corresponding to a $\pm 1\sigma$ confidence interval. The number of grains extracted from each thin section is also shown.

2.2. Fabric evolution

As shown in Fig. 2, the fabric evolution is characterized by a strengthening with increasing depth from a near-isotropic distribution of **c**-axes at 18 m, to a very strongly concentrated vertical single maximum. Fig. 2 also represents the evolution with depth of the isotopic signal (Stenni and co authors, 2011). A change in the rate of strengthening of the fabrics appears between 750 m and 900 m, which corresponds to the Antarctic Cold Reversal and the climatic transition to the last glacial period. Another change occurs close to 950 m depth with a stagnation of the fabric strengthening, down to about 1200 m where a sharp strengthening of the fabric takes place, toward a saturation close to the limit that can be reached for a polycrystalline ice (very close to a uniform orientation in only one direction). This abrupt change is in phase with the AIM 12 (Antarctic Isotope Maximum) cooling measured in the isotopic data (Stenni and co authors, 2011).

The discontinuity at 1171 m depth (arrow in Fig. 2) in the orientation tensor eigenvalues can be attributed to a few big grains with orientations at about 40 to 50° away from the single maximum (see Fig. 3). A similar observation is done at 1411 m depth (arrow in Fig. 2) (see Fig. 4). Then, below about 1450 m the fabric strength decreases, in phase with the transition that leads to the last interglacial and to older cycles, too much compressed to be clearly identified.

Fig. 4 represents the evolution of the microstructures and the fabrics in the range 1361 - 1581 m (grey area in Fig. 2). Fabrics and microstructures from 1200 to 1361 m are very similar to those from 1361 to 1381 m. From 1411 m down to 1500 m depth, however, an increasing number of grains with

orientations departing from the single maximum appear. These orientations explain the progressive decrease of the fabric strength, although the fabric remains dominated by a strong single maximum. The bottom part of the core is characterized by a transition to very large grain size ice (up to 40-50 cm) occurring between 1481 m and 1500 m. From this depth, owing to the low number of grains in each thin section, the measurements have no more statistical meaning and are not represented in the figures.

2.3. Grain size evolution

Grain size evolution down to 1481 m depth is shown in Fig. 5 together with the dust content evolution extracted from (Delmonte et al., 2010). Fig. 6 presents the grain size evolution with the ice age, extracted from the TALDICE-1 chronology (Buiron et al., 2011). The focus on the first 30 000 years (first 950 m) shows a trend similar to the one measured along the first 1500 m of the GRIP ice core (Thorsteinsson et al., 1997) or the first 1000 m of the Byrd ice core (Alley et al., 1995) with a grain size increase followed by an average stabilization. The stabilization is around a value of 2.1 mm between 350 and 950 m depth. The theoretical normal grain growth law which predicts a grain size increase following the Eq. (8) (Gow, 1969) was applied to the data down to 5600 years.

$$D^2 = {D_0}^2 + K \times t \tag{8}$$

with D the mean grain size, D_0 the initial mean grain size, K the grain boundary migration rate.

A good match is found with a grain boundary migration rate $K = 6.9 \times 10^{-10}$ $m^2 yr^{-1}$ (R^2 coefficient of 0.9). This value is about five times lower than

the rate measured at GRIP ($K = 3.8 \times 10^{-9}\ m^2 yr^{-1}$) where the surface temperature is -32°C (against -41°C at Talos Dome) and the average grain size 4 mm.

Around this mean value of 2.1 mm, the grain size variability is quite high. This is coherent with the dust content variability in this range (see Fig. 5). The LGM/Holocene dust concentration ratio is about 12 at Talos Dome (Delmonte et al., 2010), compared with more than 50 at EPICA Dome C (Lambert et al., 2008) where the correlation between grain size and dust concentration is stronger (Durand et al., 2006b).

3. Modeling the fabric evolution using a ViscoPlastic Self-Consistent scheme

Following pioneer work of Castelnau et al. (1996b, 1998) on the GRIP ice core, we applied a ViscoPlastic Self Consistent model to represent the fabric evolution along the Talos Dome ice core.

3.1. The VPSC scheme adapted to ice

The VPSC formulation, also known as a "mean-field" approach, is based on a statistical description of the microstructure of polycrystalline aggregates. Grains exhibiting the same crystallographic orientation are treated as a single "mechanical phase". Each phase is embedded in an infinite homogeneous medium with the same mechanical behavior as the polycrystal. The self-consistent (SC) approximation used to estimate the mechanical response of polycrystals was originally developed for linear elastic materials (Hershey, 1954). The key benefit of this method is the estimation of the stress and strain localization within each phase (a phase represents all grains

with the same orientation), in relation with the microstructure (orientation distribution) and the boundary conditions.

In the ViscoPlastic SC approaches, the problem is solved by finding an equilibrated stress field related to a compatible strain field, which is adapted to the local constitutive relation that describes the non-linear viscoplastic deformation at the grain scale (Molinari et al., 1987).

Ice deformation occurs in such a non-linear viscoplastic regime, characterized by a Glen flow law (9) (Glen, 1955) that associates the effective strain rate ($\dot{\varepsilon}$) to the effective stress (σ) with a stress exponent n varying between 2 and 3.

$$\dot{\varepsilon} = B \times \sigma^n, \tag{9}$$

with B a parameter following an Arrhenius dependence on the temperature. For nonlinear aggregates like ice, the SC scheme is applied by providing a local linearization of the mechanical behavior, in order to reduce the problem to the case of the well-constrained thermo-elasticity (Molinari et al., 1987). The obtained mechanical behavior is therefore an approximation that strongly depends on the linearization approach (Ponte-Castañeda and Suquet, 1998).

Castelnau et al. (1996b) applied the tangent version of the linearization scheme developed by Lebensohn and Tomé (1993) to simulate the fabric development along the GRIP ice core. Since then, it was shown that the tangent prediction strongly overestimates the fabric development (Wenk and Tomé, 1999). It suffers from significant inconsistencies (Gilormini, 1995; Masson et al., 2000) that lead to a significant underestimation of the effective viscosity for materials with a large viscoplastic anisotropy such as ice (with

only one easy slip system for dislocations, the basal system).

The second-order linearization scheme (SO) proposed by Liu and Castañeda (2004), was shown to provide the better mechanical response, in comparison with full-field approaches that integrate real microstructures. For polycrystals with a strong viscoplastic anisotropy, strong deformation gradients are likely to develop inside grains owing to the contrast of properties between neighboring grains. The second-order approach takes into account a statistical representation of these intragranular fluctuations by incorporating the field fluctuations at the grain scale in the linearization procedure (Liu and Castañeda, 2004). Such an improvement appears essential to provide a good representation of the mechanical behavior of materials with a high viscoplastic anisotropy such as ice.

This VPSC-SO model was selected to simulate the fabric development along the Talos Dome ice core. A polycrystal with 500 grains (or mechanical phases) of the same size (the absolute value has no impact as there is no length scale in the code), deforms by dislocation glide on basal, prismatic and pyramidal slip systems as in Castelnau et al. (1996b). Dynamic recrystallization mechanisms are not taken into account in this formulation.

The rheological behavior at the grain scale is given by a standard power law

$$\dot{\gamma}_{(k)} = \dot{\gamma}_0 \left| \frac{\tau_{(k)}}{\tau_{0(k)}} \right|^{n-1} \frac{\tau_{(k)}}{\tau_{0(k)}}, \tag{10}$$

with $\dot{\gamma}_{(k)}$ the rate of slip on slip system (k), $\tau_{(k)}$ the shear stress, and $\tau_{0(k)}$ the critical shear stress necessary to activate slip on the system k. The classical $n = 3$ value was adopted for the stress sensitivity (Castelnau et al.,

1996b,a, 1997). The basal, prismatic and pyramidal systems were assigned the respective critical stresses τ_0, $50 \times \tau_0$ and $50 \times \tau_0$ (τ_0 is an arbitrary reference stress). This critical stress is the minimum resolved stress on the slip system necessary to induce slip on this system. The basal slip is therefore 50 times easier to activate than the prismatic and pyramidal slips. These parameters were adjusted to accurately reproduce the anisotropic viscoplastic response of the ice polycrystal following Castelnau et al. (1996b,a, 1997).

3.2. Modeling of the fabric evolution

The run was performed assuming a vertical compression under a uniform strain rate of 10^{-12} s^{-1}, based on an accumulation rate estimation of 8 cm ice/yr.

In order to compare measured and simulated fabric data, their evolutions are represented as a function of the cumulated compressive strain. In the specific case of a perfect dome, the ice is supposed to deform mainly by compression along the vertical direction. The cumulated compressive strain is then directly linked to the thinning of a layer by:

$$\overline{\varepsilon}_c = \frac{a}{a_0} - 1, \tag{11}$$

with a the thickness of a layer of initial thickness a_0. The cumulated compressive strain evolution, as a function of depth, was deduced from the thinning function provided by the TALDICE-1 chronology (Buiron et al., 2011). For this chronology, the thinning function is provided for a given scenario of the evolution of the accumulation rate. The first scenario for the accumulation rate is obtained from isotopic data, and the thinning function is first estimated from a 1-D flow model following Parrenin et al. (2007). Both are later

adjusted using the inverse method of Lemieux-Dudon et al. (2010) which generates an optimal compromise between the a priori scenario provided by the flow model and the chronological information from different time markers.

Fig. 8 represents the modeled and measured fabric evolutions as a function of the cumulated compressive strain, and the evolution of this strain with depth. To estimate the impact of an initial anisotropic fabric in firn on the global fabric evolution, initial eigenvalue inputs were allowed to vary around the value measured at 18 m depth (see section 2.3). Dashed lines in Fig. 8 represent the range between an isotropic initial fabric and an anisotropy slightly higher than the one measured in the firn.

Although shear could affect the deformation along the core, it was not included in the simulation for several reasons. First of all, the mechanical scheme of the VPSC approach requires the activation of at least four independent slip systems (see Eq. (10)), with a slight amount of non-basal slip. For the specific conditions of simple shear, this non-basal slip has a strong impact on the macroscopic behavior. Because of this necessary non-basal activity, the model is unable to predict the fabrics measured in conditions of shear, that are characterized by a strong single maximum perpendicular to the shear plane (Hudleston, 1977; Bouchez and Duval, 1982; Wenk and Tomé, 1999). Similar conclusions were reached for olivine, which mechanical behavior is highly anisotropic, similarly to ice (Zhang and Karato, 1995; Tommasi et al., 2000). Secondly, the purpose of this modeling exercise is not to strictly reproduce the measured fabric evolution, as a 3D configuration would be required to integrate the exact flow conditions (with exact boundary constraints) (Gillet-Chaulet et al., 2006; Martín et al., 2009) but rather

to highlight the inaccuracies arising from the assumption of a perfect dome.

4. Result analyses

4.1. Fabric and grain size evolution

The global trend of the c-axis strengthening along the Talos Dome core compares qualitatively well with the one measured along the EPICA Dome C, the GRIP or the Dome Fuji cores (Thorsteinsson et al., 1997; Azuma et al., 1999; Wang et al., 2003; Durand et al., 2009). This type of fabric evolution is coherent with a first order influence of a dominating compressive strain along the core. Nevertheless, clear departures from this trend are visible, which we will try to analyze in the following part.

We have measured fabrics that are not isotropic in firn samples, as high as technically possible with non-impregnated samples, i.e. up to 18 m depth. Similar observations were done along the Siple Dome ice core (Diprinzio et al., 2005) and the EPICA Dome C ice core (Durand et al., 2009). At 18 m depth, in the Talos Dome coring site, a compressive strain of less than 1% is expected from the TALDICE-1 thinning function. With isotropic initial conditions, the $a_1^{(2)}$ eigenvalue of the orientation tensor predicted by the VPSC-SO model after 1% of deformation is about 0.35. The $a_1^{(2)}$ eigenvalue measured at 18 m is 0.39 (0.40 at 28 m and 0.44 at 48 m), clearly higher than the 0.35 value predicted, and 7% of compressive strain is required to reach 0.39 with the VPSC-SO model (see Fig. 8).

To our knowledge, there exist no detailed analyses of the link between densification processes and fabric evolution, but only isolated data of fabric measurements along firn cores (Spaulding et al., 2011). From Arnaud

et al. (1998, 2000), between about 5 to 20 m depth and for conditions similar to the Talos Dome site, densification is expected to be isothermal, and the main process is believed to be re-arrangement by grain boundary sliding. No preferred orientation is expected to occur during such process. Closer to the surface, temperature gradient metamorphism dominates the grain size evolution, and the impact on fabric development has only been seldom investigated (Carns et al., 2010). From observation of individual snow crystals, Adams and Miller (2003) made the hypothesis that, during temperature gradient metamorphism, there could exist favored orientation growth which depends on the conditions of the metamorphism (temperature range, level of supersaturation, ice-grain/pore space). High resolution fabric measurements in firn are therefore necessary to better explain this measured anisotropy, but it has to be taken into account, especially when modeling the fabric evolution.

In the first 350 m of the core, the grain size evolution well matches a normal grain growth law as measured along the GRIP and Byrd ice cores. Then, the average grain size stabilizes around 2.1 mm down to about 950 m. The continuous DRX model suggested by de la Chapelle et al. (1998); Montagnat and Duval (2000) therefore applies in the central part of this core. Continuous DRX mechanism is supposed to slow the fabric strengthening. Indeed, the associated nucleation mechanism (by progressive misorientation of sub-boundaries) is supposed to slightly open the fabrics (Wenk et al., 1997; Castelnau et al., 1996b), and the associated grain boundary migration reduces the deformation stored energy.

Local discontinuous DRX events were observed at 1171 m depth (Fig. 3),

with isolated grains of size bigger than the average, and orientation deviating from the main orientation direction, and at several other depths below 1400 m. The big grain sizes are explained by a rapid grain boundary migration, and the obvious departure from the average grain orientation results from new grain nucleations (de la Chapelle et al., 1998). The 10 m sampling of the fabric measurements probably prevents the observation of further localized discontinuous DRX events. These events are the signature of a highly heteregeneous state of stress at the origin of a local level of strain high enough to induce nucleation and fast grain boundary migration. Nevertheless, down to 1500 m depth, the localized events of discontinuous DRX do not drastically change the fabric toward isotropy or multiple maxima as observed along the Siple Dome ice core (Diprinzio et al., 2005), and in the bottom of the GRIP ice core (Thorsteinsson et al., 1997) for instance.

The fabric evolution tendency shows a break, with a higher strengthening rate below 750 m and continuing down to 900 m depth. This depth range corresponds to the Holocene - Wisconsin transition. Following Durand et al. (2007), this faster fabric strengthening could be explained by the associated impact of a change in ice viscosity due to the glacial-interglacial transition and of the progressive influence of a shear stress component.

Along ice cores, thinning is only controlled by the compressive strain (Paterson, 1991). As extrusion flow can not occur, two layers with different viscosity will experience the same amount of thinning. On the other hand, shearing by itself will not produce any thinning but will strongly enhance fabric strengthening. As currently observed along ice cores, smaller grain

sizes and strengthened fabrics are measured in glacial ice with respect to interglacial ice (see for instance de la Chapelle et al. (1998); Diprinzio et al. (2005); Durand et al. (2006b, 2009)). The higher fabric strengthening rate measured in the glacial ice layer of the Talos Dome ice core confirms the occurrence of a positive feedback with glacial ice layer experiencing more shear, so that its fabric gets more clustered and then softer for shear (Paterson, 1991).

Between 950 m and 1150 m depth, the fabric is constant, with similar fabrics in adjacent layers. Here we provide two possible analyses. The first one considers that these adjacent layers could have experienced the same deformation history (same flow) but with different initial viscosities. They would therefore be differently influenced by the shear stress, and end up with very similar fabrics at adjacent depths. The dust level measured in this range of depth is highly variable (see Fig. 5), and about twice to five times higher than during the Holocene (Delmonte et al., 2010). The high variability of dust content during this period could induce variability in the viscosity between adjacent layers from the very top of the core. The second explanation could be related to some changes in the dome configuration during the corresponding period of time. In this case, the layers would have experienced different, but close, deformation histories. Urbini et al. (2008) showed that variations in the accumulation rate during the last few centuries could have resulted in some dome summit migration. Although highly speculative, such an explanation could also hold for this anomaly in the fabric evolution.

4.2. Comparison with the fabric evolution along the EPICA Dome C ice core

The EPICA Dome C ice core was drilled at Dome C, in Antarctica (75° 06'S, 123° 21'E) down to 3259.72 m depth. Owing to the low accumulation observed in this inland site of Antarctica, the upper 3139 m of the core provide about 800 000 years of climatic records (Jouzel et al., 2007).

Because of the difference in depth (and age) between the two ice cores, a direct comparison between them on a depth scale cannot be done; however, they can be compared on a scale of cumulated compressive strain. For EPICA Dome C, we used the EDC3 chronology from Parrenin et al. (2007) to obtain the cumulated compressive strain as a function of depth, following Eq. 11. The fabric data along the EPICA Dome C core are given by (Durand et al., 2009).

Talos Dome and EPICA Dome C fabrics show very similar evolutions, when compared as a function of cumulated compressive strain, see Fig. 7. Since the overall location and conditions at the two coring sites are much different, such a comparison tends to demonstrate that the cumulated compressive strain is the main parameter controlling the fabric strengthening. In particular, one can note that the fabric evolution changes measured at 1750 m along the EPICA Dome C core (Durand et al., 2007) and at 750 m along the Talos Dome core occur for the same cumulated compressive strain of about 0.6. Both depths correspond to climatic changes from glacial to interglacial conditions but at different times. The feedback between changes in layer viscosity (probably related with variation in dust content) and shear stress would then mainly affect the fabric evolution after a given level of fabric anisotropy is reached, and therefore after a given amount of cumulated

compressive strain.

4.3. Comparison between the measured and the simulated fabric evolution.

The modeling of fabric evolution under the assumption of uniaxial compression at constant strain rate represents well the configuration of a perfect dome. The comparison between simulation and measurements thus allows to identify the departures from this ideal state of strain.

Fig. 8 shows that the model provides a good overall estimate of the fabric evolution trend, especially when a non isotropic initial fabric is considered according to the measurements.

Since continuous dynamic recrystallization processes, as expected along the core (section 2.3), are not represented in the VPSC-SO scheme adopted here, the slight overestimation of the fabric strengthening in the range 350 to 950 m depth (strain from ≈ 0.25 to 0.7) was expected (Castelnau et al., 1996b; de la Chapelle et al., 1998; Thorsteinsson, 2002).

Below 950 m depth (strain ≈ 0.75), the measured fabric is much stronger than the modeled fabric, and the rate of fabric strengthening from strain of ≈ 0.6 (about 750 m depth) can not be reproduced by the model under the hypothesis of uniaxal compression. This comparison therefore reinforces the assumption made in section 4.1 of the influence of a shear stress component on the fabric strengthening. In particular, the shear stress would be responsible for the fabric strengthening below 750 m (strain ≈ 0.6), and for the strong c-axis clustering below 950 m depth.

5. Concluding remarks

The fabric evolution measured along the Talos Dome ice core is characterized by a strengthening toward the vertical direction, very similar to the one measured along several other Greenland and Antarctic cores, where the main deformation component is vertical compression. Nevertheless, variations in the c-axis clustering rate are observed at locations corresponding to the climatic transitions.

In particular, an increase in the rate of fabric strengthening is observed in the depth range covering the Last Glacial Maximum - Holocene transition. The influence of a shear component of stress associated with viscosity changes between successive layers is therefore suggested, following (Durand et al., 2007). This hypothesis is strengthened by the comparison performed between the measured fabric evolution and the one simulated under the assumption of a "perfect dome", using the VPSC-SO mean-field approach. Under the perfect dome assumption, i.e. under uniaxial compression at a constant rate, the model can not represent the strength of the fabrics measured below 950 m depth, that could be explained by a non negligible shear stress.

Above 750 m depth, the simulation provides a qualitative good match with the measured fabrics, providing that (i) we enter a non-isotropic fabric in the top layer, similar to the one measured in the firn, and (ii) we explain the slight overestimation between 350 m and 750 m depth by continuous DRX not being taken into account in the model. Although continuous DRX was probably active in the lower part of the core, we loose track of it because of the shear-induced fabric strengthening.

Indeed, the analysis of the grain size evolution measurements, associated

with the fabric data, highlights the occurrence of dynamic recrystallization processes. The first part of the core, above 950 m depth, is dominated by normal grain growth and continuous DRX, while discontinuous DRX is only observed locally at various depths below 1170 m. Discontinuous DRX does not seem to influence the fabric evolution down to 1400 m.

6. Acknowledgements

TAlos Dome ICE core project (TALDICE), a joint European program led by Italy, is funded by national contributions from Italy, France, Germany, Switzerland and the United Kingdom. The main logistical support was provided by PNRA at Talos Dome. We thank the logistic and drilling TALDICE team for their efficiency over each drilling season. Funding support for the laboratory measurements and dating work was provided by the Institut INSU of CNRS through its program LEFE. Many thanks to Hugh Corr who provided the radar images (BAS/PNRA collaboration in 2005/06). We thank Ricardo Lebensohn and Carlos Tomé from LANL (USA) for the access to the VPSC7 code, and Paul Duval, Gaël Durand, Fabien Gillet-Chaulet and Olivier Gagliardini from LGGE for fruitful discussions. This is TALDICE publication no 26.

References

Adams, E., Miller, D., 2003. Ice crystals grown from vapor onto an orientated substrate: application to snow depth-hoar development and gas inclusions in lake ice. J. Glaciol. 49, 8–12.

Alley, R.B., 1988. Fabrics in polar ice sheets - Development and prediction. Science 240, 493–495.

Alley, R.B., Gow, A.J., Meese, D.A., 1995. Mapping c-axis fabrics to study physical processes in ice. J. Glaciol. 41.

Anderson, M.P., Grest, G.S., Srolovitz, D.J., 1989. Computer simulation of normal grain growth in three dimensions. Philos. Mag. B 59, 293–329.

Arnaud, L., Lipenkov, V., Barnola, J., Gay, M., Duval, P., 1998. Modelling of the densification of polar firn: characterization of the snow-firn transitions. Ann. Glaciol. 26, 39–44.

Arnaud, L., Weiss, J., Gay, M., Duval, P., 2000. Shallow-ice microstructure at Dome Concordia. Ann. Glaciol. 30, 8–12.

Azuma, N., Wang, Y., Mori, K., Narita, H., Hondoh, T., Shoji, H., Watanabe, O., 1999. Textures and fabrics in the Dome F (Antarctica) ice core. Ann. Glaciol. 29, 163–168.

Bianchi, C., Cafarella, L., De Michelis, P., Forieri, A., Frezzotti, M., Tabacco, I.E., Zirizzotti, A., 2003. Radio Echo Sounding (RES) investigations at Talos Dome (East Antarctica): bedrock topography and ice thickness. Ann. Geophysics 46, 1265–1270.

Bouchez, J.L., Duval, P., 1982. The fabric of polycrystalline ice deformed in simple shear : experiments in torsion, natural deformation and geometrical interpretation. Textures and microstructures 5, 171–190.

563 Buiron, D., Chappellaz, J., Stenni, B., Frezzoti, M., Baumgartner, M.,
564 Capron, E., Landais, A., Lemieux-Dudon, B., Masson-Delmotte, V., Mon-
565 tagnat, M., Parrenin, F., Schilt, A., 2011. TALDICE-1 age scale of the
566 Talos Dome deep ice core, East Antarctica. Climate of the Past 7, 1–16.

567 Carns, R., Waddington, E.D., Pettit, E.C., Warren, S.G., 2010. A Model
568 of Grain Growth and Crystal Fabric in Polar Snow and Firn. AGU Fall
569 Meet. Abs. , D572.

570 Castelnau, O., Canova, G.R., Lebensohn, R.A., Duval, P., 1997. Modelling
571 viscoplastic behavior of anisotropic polycrystalline ice with a self-consistent
572 approach. Acta Mater. 45, 4823 – 4834.

573 Castelnau, O., Duval, P., Lebensohn, R.A., Canova, G., 1996a. Viscoplas-
574 tic modeling of texture development in polycrystalline ice with a self-
575 consistent approach : Comparison with bound estimates. J. Geophys.
576 Res. 101, 13,851–13,868.

577 Castelnau, O., Shoji, H., Mangeney, A., Milsch, H., Duval, P., Miyamoto,
578 A., Kawada, K., Watanabe, O., 1998. Anisotropic behavior of GRIP ices
579 and flow in Central Greenland. Earth Planet. Sc. Lett. 154, 307 – 322.

580 Castelnau, O., Thorsteinsson, T., Kipfstuhl, J., Duval, P., Canova, G.R.,
581 1996b. Modelling fabric development along the GRIP ice core, central
582 Greenland. Ann. Glaciol. 23, 194–201.

583 de la Chapelle, S., Castelnau, O., Lipenkov, V., Duval, P., 1998. Dynamic
584 recrystallization and texture development in ice as revealed by the study

of deep ice cores in Antarctica and Greenland. J. Geophys. Res. 103, 5091–5105.

Delmonte, B., Baroni, C., Andersson, P.S., Schoberg, H., Hansson, M., Aciego, S., Petit, J.R., Albani, S., Mazzola, C., Maggi, V., Frezzotti, M., 2010. Aeolian dust in the Talos Dome ice core (East Antarctica, Pacific/Ross Sea sector): Victoria Land versus remote sources over the last two climate cycles. J. Quaternary Sci. 25, 1327–1337.

Diprinzio, C.L., Wilen, L.A., Alley, R.B., Fitzpatrick, J.J., Spencer, M.K., Gow, A.J., 2005. Fabric and texture at Siple Dome, Antarctica. J. Glaciol. 51, 281–290.

Durand, G., Gagliardini, O., Thorsteinsson, T., Svensson, A., Kipfstuhl, J., Dahl-Jensen, D., 2006a. Ice microstructure and fabric: an up to date approach to measure textures. J. Glaciol. 52, 619–630.

Durand, G., Gillet-Chaulet, F., Svensson, A., Gagliardini, O., Kipfstuhl, S., Meyssonnier, J., Parrenin, F., Duval, P., Dahl-Jensen, D., Azuma, N., 2007. Change of the ice rheology with climatic transitions. Implication on ice flow modelling and dating of the EPICA Dome C core. Clim. Past 3, 155–167.

Durand, G., Svensson, A., Persson, A., Gagliardini, O., Gillet-Chaulet, F., Sjolte, J., Montagnat, M., Dahl-Jensen, D., 2009. Evolution of the texture along the EPICA Dome C ice core. Supp. Issue Low Temp. Sci. 68, 91–106.

Durand, G., Weiss, J., Lipenkov, V., Barnola, J., Krinner, G., Parrenin, F., Delmonte, B., Ritz, C., Duval, P., Röthlisberger, R., Bigler, M., 2006b.

608 Effect of impurities on grain growth in cold ice sheets. J. Geophys. Res.
609 111, F01015.

610 Efron, B., Tibshirani, R., 1993. An introduction to the bootstrap. Chapman
611 and Hall.

612 Frezzotti, M., Urbini, S., Proposito, M., Scarchilli, C., Gandolfi, S., 2007.
613 Spatial and temporal variability of surface mass balance near Talos Dome,
614 East Antarctica. Geophys. Res. Let. - Earth Surface 112 (F02032), 1 – 15.

615 Gagliardini, O., Durand, G., Wang, Y., 2004. Grain area as a statistical
616 weight for polycrystal constituents. J. Glaciol. 50, 87–95.

617 Gillet-Chaulet, F., Gagliardini, O., Meyssonnier, J., Zwinger, T., Ruoko-
618 lainen, J., 2006. Flow-induced anisotropy in polar ice and related ice-sheet
619 flow modelling. J. Non-Newtonian Fluid Mech. 134, 33–43.

620 Gilormini, P., 1995. A critical evaluation for various non-linear extensions
621 of the self-consistent model., in: Pineau, A., Zaoui, A. (Eds.), IUTAM
622 Symp. on Michromecanics of Plasticity and Damage of Multiphase Mate-
623 rials, Klower Acad. Publ., Sèvres, France. pp. 67–74.

624 Glen, J., 1955. The creep of polycrystalline ice. Proc. Roy. Soc. London
625 A228, 519–538.

626 Gow, A., 1969. On the rate of growth of grains and crystals in south polar
627 firn. J. Glaciol. 8, 241–252.

628 Gow, A.J., Williamson, T.C., 1976. Rheological implications of the internal

629 structure and crystal fabrics of the West Antarctic ice sheet as revealed
630 by deep core drilling at Byrd station. Geol. Soc. Am. Bull. 87, 1665–1677.

631 Hershey, A.V., 1954. The elasticity of an isotropic aggregate of anisotropic
632 cubic crystals. J. Appl. Mech. 21, 236–240.

633 Hudleston, P.J., 1977. Progressive development of fabrics across zones of
634 shear in glacial ice, in: Saxena, S.K., Bhattacharji, S. (Eds.), Energetics
635 of Geological Processes, Springer-Verlag, New York. pp. 121–150.

636 Humphreys, F.J., Hatherly, M., 2004. Recrystallization and related annealing
637 phenomena. Pergamon, Oxford. Second edition.

638 Jouzel, J., Masson-Delmotte, V., Cattani, O., Dreyfus, G., Falourd, S., Hoff-
639 mann, G., Minster, B., Nouet, J., Barnola, J.M., Chappellaz, J., Fischer,
640 H., Gallet, J.C., Johnsen, S., Leuenberger, M., Loulergue, L., Luethi, D.,
641 Oerter, H., Parrenin, F., Raisbeck, G., Raynaud, D., Schilt, A., Schwan-
642 der, J., Selmo, E., Souchez, R., Spahni, R., Stauffer, B., Steffensen, J.P.,
643 Stenni, B., Stocker, T.F., Tison, J.L., Werner, M., Wolff, E.W., 2007. Or-
644 bital and Millennial Antarctic Climate Variability over the Past 800,000
645 Years. Science 317, 793–796.

646 Lambert, F., Delmonte, B., Petit, J.R., Bigler, M., Kaufmann, P.R., Hutterli,
647 M.A., Stocker, T.F., Ruth, U., Steffensen, J.P., Maggi, V., 2008. New
648 constraints on the aeolian dust cycle from a 800,000-year Antarctic ice
649 core record. Nature 452, 616–619.

650 Lebensohn, R.A., Tomé, C.N., 1993. A self-consistent viscoplastic model:

651 prediction of rolling textures of anisotropic polycrystals. Mat. Sci. and
652 Engin., A 175, 71–82.

653 Lebensohn, R.A., Tomé, C.N., Ponte Castañeda, P., 2005. Improving the self-
654 consistent predictions of texture development of polycrystals incorporating
655 intragranular field fluctuations. Mater. Sci. Forum 955, 495–497.

656 Lemieux-Dudon, B., Blayo, E., Petit, J.R., Waelbroeck, C., Svensson, A.,
657 Ritz, C., Barnola, J.M., Narcisi, B.M., Parrenin, F., 2010. Consistent
658 dating for Antarctic and Greenland ice cores. Quaternary Sci. Rev. 29, 8
659 – 20.

660 Liu, Y., Castañeda, P.P., 2004. Second-order theory for the effective behavior
661 and field fluctuations in viscoplastic polycrystals. Journal of the Mechanics
662 and Physics of Solids 52, 467 – 495.

663 Martín, C., Gudmundsson, G.H., Pritchard, H.D., Gagliardini, O., 2009. On
664 the effects of anisotropic rheology on ice flow, internal structure, and the
665 age-depth relationship at ice divides. J. Geophys. Res. 114, F04001.

666 Masson, R., Bornert, M., Suquet, P., Zaoui, A., 2000. An affine formulation
667 for the prediction of the effective properties of nonlinear composites and
668 polycrystals. J. Mech. and Phys. Solids 48, 1203 – 1227.

669 Molinari, A., Canova, G., Ahzi, S., 1987. A self-consistent approach of the
670 large deformation polycrystal viscoplasticity. Acta. Metall. 35, 2983–2994.

671 Montagnat, M., Duval, P., 2000. Rate controlling processes in the creep of
672 polar ice, influence of grain boundary migration associated with recrystal-
673 lization. Earth Planet. Sc. Lett. 183, 179–186.

Palm, R., 2002. Utilisation du bootstrap pour les problèmes statistiques liés à l'estimation des paramètres. Biotechnol. Agron. Soc. Environ. 6, 143–153.

Parrenin, F., Barnola, J.M., Beer, J., Blunier, T., Castellano, E., Chappellaz, J., Dreyfus, G., Fischer, H., Fujita, S., Jouzel, J., Kawamura, K., Lemieux-Dudon, B., Loulergue, L., Masson-Delmotte, V., Narcisi, B., Petit, J.R., Raisbeck, G., Raynaud, D., Ruth, U., Schwander, J., Severi, M., Spahni, R., Steffensen, J.P., Svensson, A., Udisti, R., Waelbroeck, C., Wolff, E., 2007. The EDC3 chronology for the EPICA Dome C ice core. Clim. Past 3, 575–606.

Paterson, W.S.B., 1991. Why ice-age ice is sometimes soft. Cold Reg. Sci. Technol. 20, 75–98.

Paterson, W.S.B., 1994. The physics of glaciers. Pergamon, Oxford.

Peternell, M., Russell-Head, D., Wilson, C., 2011. A technique for recording polycrystalline structure and orientation during in situ deformation cycles of rock analogues using an automated fabric analyser. J. Microsc. 242, 181–188.

Pettit, E.C., Thorsteinsson, T., Jacobson, P., Waddington, E.D., 2007. The role of crystal fabric in flow near an ice divide. J. Glaciol. 53, 277–288.

Pettit, E.C., Waddington, E.D., Harrison, W.D., Thorsteinsson, T., Elsberg, D., Morack, J., Zumberge, M.A., 2011. The crossover stress, anisotropy and the ice flow law at Siple Dome, West Antarctica. J. Glaciol. 57, 39–52.

Ponte-Castañeda, P., Suquet, P., 1998. Nonlinear composites. Adv. App. Mech. 34, 171–302.

Russell-Head, D.S., Wilson, C.J.L., 2001. Automated fabric analyser system for quartz and ice. J. Glaciol. 24, 117–130.

Seddik, H., Greeve, R., Placidi, L., Hamann, I., Gagliardini, O., 2008. Application of a continuum-mechanical model for the flow of anisotropic polar ice to the EDML core, Antarctica. J. Glaciol. 54, 631–642.

Spaulding, N.E., Meese, D.A., Baker, I., 2011. Advanced microstructural characterization of four East Antarctic firn/ice cores. J. Glaciol. 57, 796–810.

Stenni, B., co authors, ., 2011. Unified antarctic and greenland climate seesaw during the last deglaciation. Science 4, 46–49.

Stenni, B., Proposito, M., Gragnani, R., Flora, O., Jouzel, J., Falourd, S., Frezzotti, M., 2002. Eight centuries of volcanic signal and climate change at Talos Dome (East Antarctica). J. Geophys. Res. 107, 4076.

Thorsteinsson, T., 2002. Fabric development with nearest-neighbor interaction and dynamic recrystallization. J. Geophys. Res. 107.

Thorsteinsson, T., Kipfstuhl, J., Miller, H., 1997. Textures and fabrics in the GRIP ice core. J. Geophys. Res. 102, 26,583–26,600.

Tommasi, A., Mainprice, D., Canova, G., Chastel, Y., 2000. Viscoplastic self-consistent and equilibrium based modeling of olivine lattice preferred orientations : Implications for the upper mantle seismic anisotropy. J. Geophys. Res. 105, 7893–7908.

718 Urbini, S., Cafarella, L., Zirizzotti, A., Bianchi, C., Tabacco, I., Frezzoti, M.,
719 2006. Location of a new ice core site at Talos Dome (East Antarctica).
720 Ann. Geophys. 49 (4/5), 1133–1138.

721 Urbini, S., Frezzotti, M., Gandolfi, S., Vincent, C., Scarchilli, C., Vittuari,
722 L., Fily, M., 2008. Historical behaviour of Dome C and Talos Dome (East
723 Antarctica) as investigated by snow accumulation and ice velocity mea-
724 surements. Global Planet. Change 60, 576 – 588.

725 Wang, Y., Kipfstuhl, S., Azuma, N., 2003. Ice fabrics study in the upper
726 1500 m of the Dome C deep ice core, East Antarctica. Ann. Glaciol. 37,
727 97 – 104.

728 Wenk, H.R., Canova, G., Bréchet, Y., Flandin, L., 1997. A deformation-
729 based model for recrystallization of anisotropic materials. Acta. Mater.
730 45, 3283–3296.

731 Wenk, H.R., Tomé, C., 1999. Modeling dynamic recrystallization of olivine
732 aggregates deformed in simple shear. J. Geophys. Res. 104, 25,513–25,527.

733 Wilson, C., Russell-Head, D., Sim, H., 2003. The application of an auto-
734 mated fabric analyzer system to the textural evolution of folded ice layers
735 in shear zones. Ann. Glaciol. 37, 7–17.

736 Zhang, S., Karato, S.I., 1995. Lattice preferred orientation of olivine aggre-
737 gates deformed in simple shear. Nature 375, 774–777.

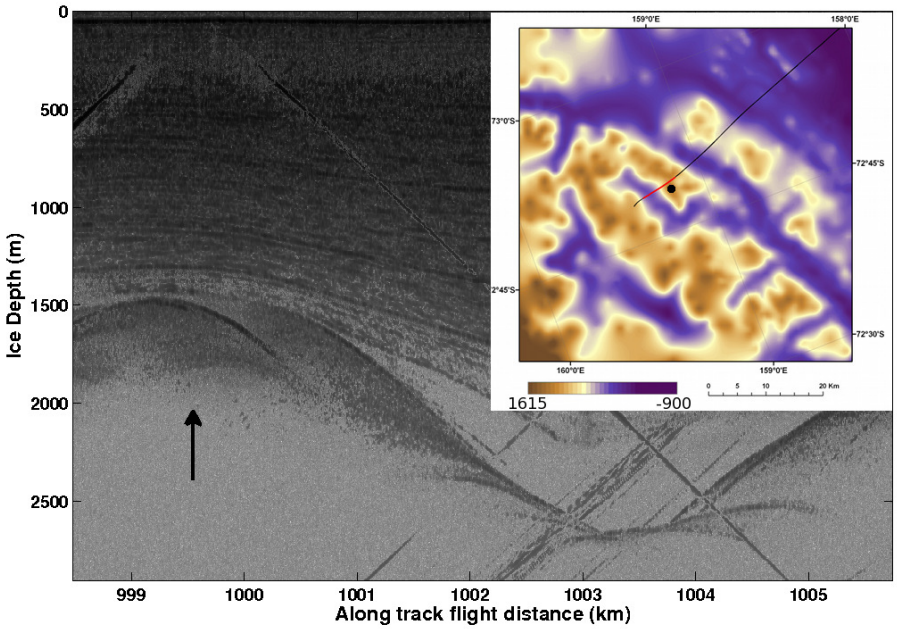

Figure 1: Radargram of the area around the Talos Dome coring site. The flight passed within 50 m from the borehole, at the position indicated by the black arrow.The inner figure represents the bedrock elevation map with the position of the coring site (black dot), the flight track followed the line (from top right), the red part being the one presented on the radargram.

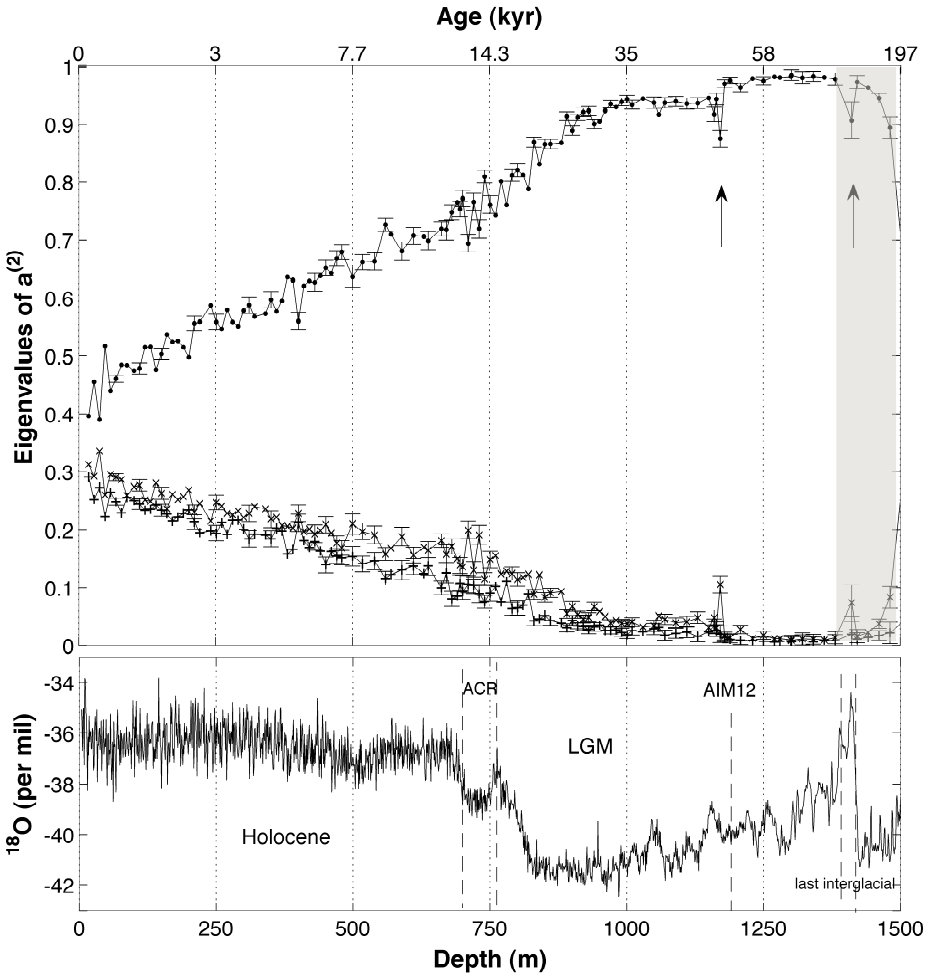

Figure 2: Orientation tensor eigenvalues along the Talos Dome core, as a function of depth (dots: $a_1^{(2)}$, crosses: $a_2^{(2)}$, plus: $a_3^{(2)}$) and ^{18}O isotope evolution as a proxy of climate changes. Error bars in the $a_i^{(2)}$ plots correspond to $\pm 1\sigma$ confidence level. The arrows show two depths with remarkable recrystallized grains, 1171 m and 1411 m. The grey area corresponds to the depth range presented in Fig. 4.

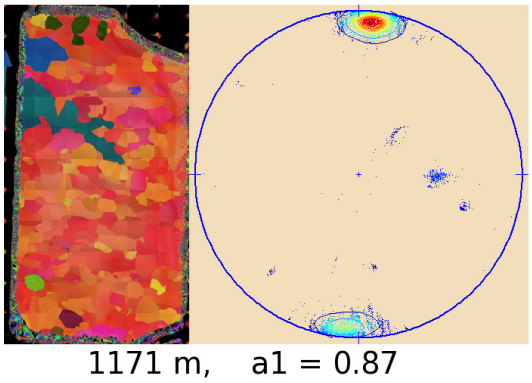

Figure 3: Microstructure in orientation color-scale and Schmidt plot obtained from the 1171 m depth thin section. In the pole figure, the blue spots out of the single maximum correspond to the orientation of the green and blue grains of the microstructure.The core vertical axis coincides with the vertical direction in the figure.

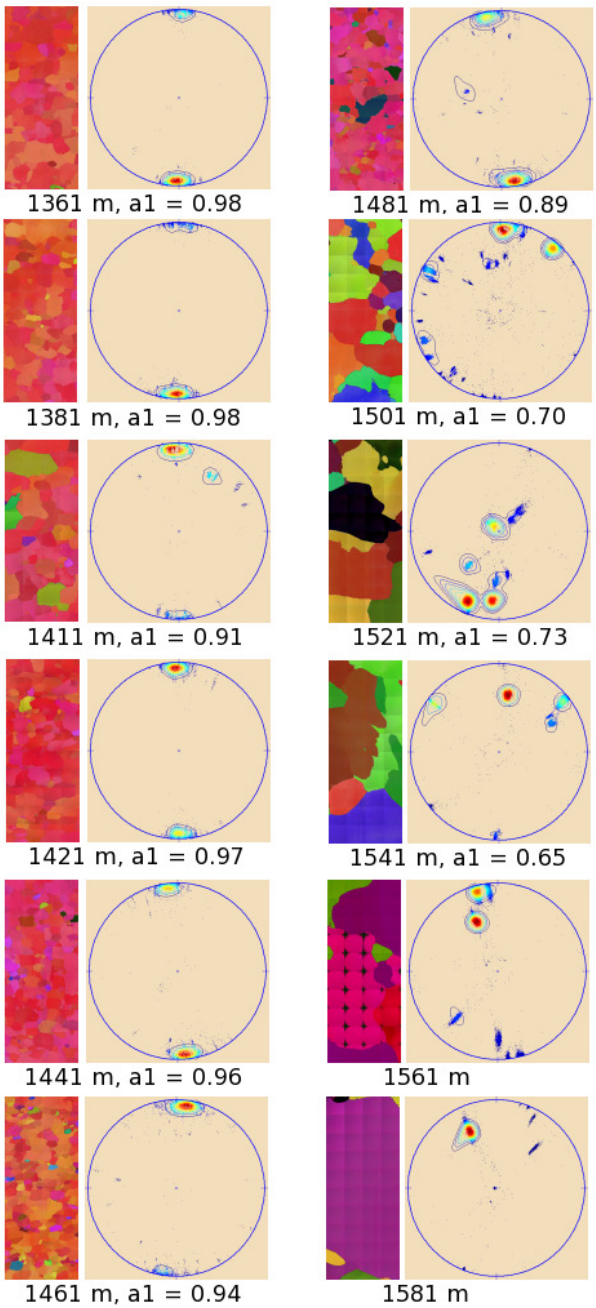

Figure 4: Microstructures in orientation color-scale and Schmidt plots obtained from 1361 m to 1581 m depth. $a_1^{(2)}$ eigenvalue is not provided after 1541 m due to the too low number of grains. The core vertical axis coincides with the vertical direction in the figure.

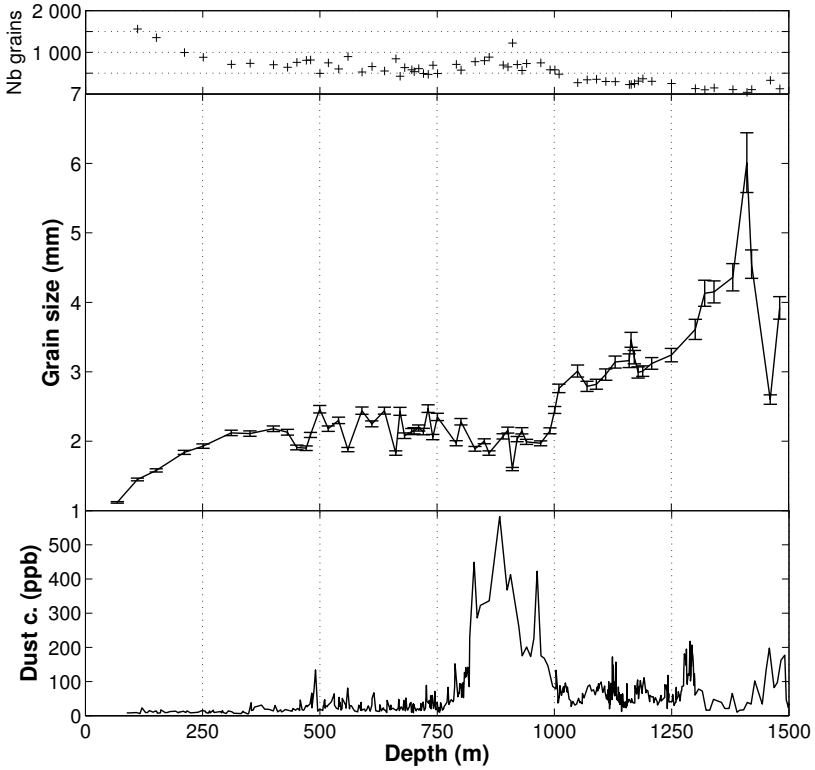

Figure 5: Average grain size (error bars correspond to $\pm 1\sigma$ confidence interval), dust content, and number of grains analyzed (in each thin section), as a function of depth along the Talos Dome ice core.

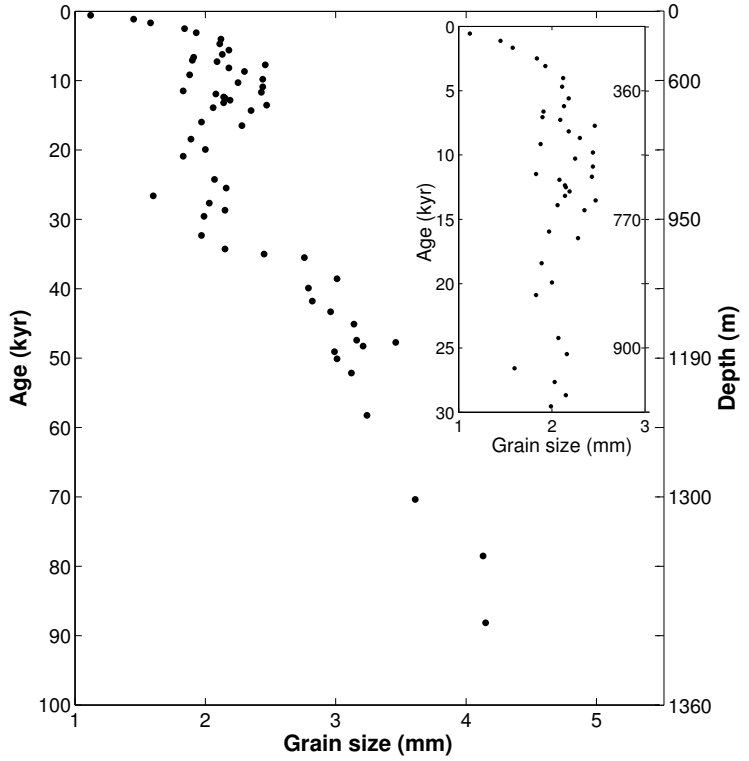

Figure 6: Average grain size as a function of ice age. The inner figure is a focus over the first 30 000 years.

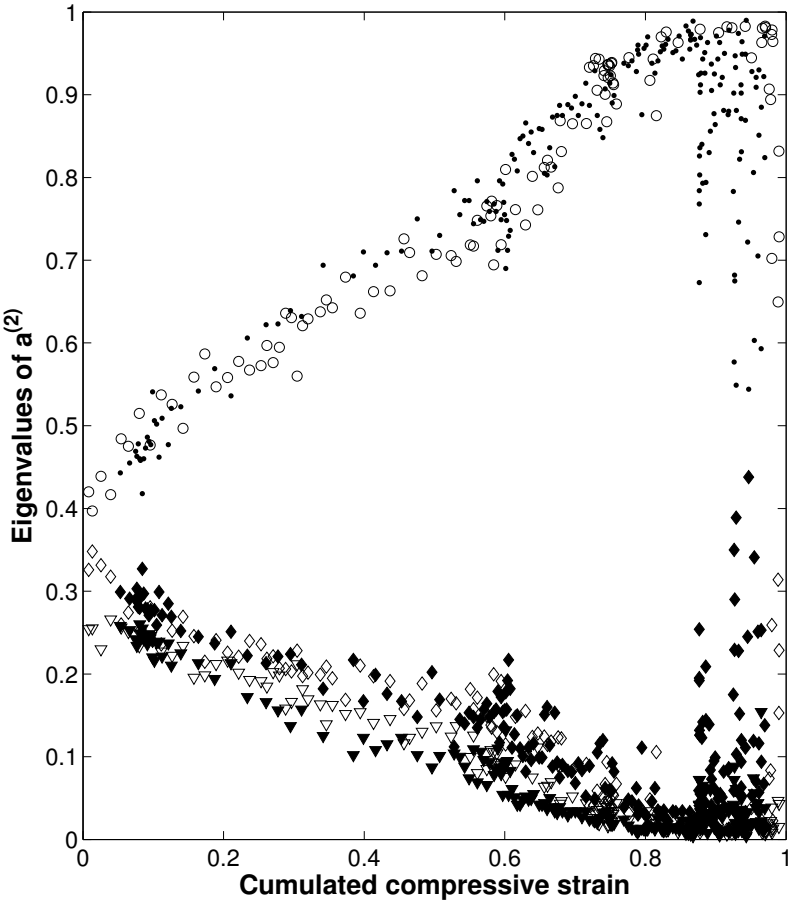

Figure 7: Eigenvalues of the orientation tensor $\mathbf{a}^{(2)}$ as a function of the cumulated compressive strain along the Talos Dome core (empty symbols) and EPICA Dome C core (full symbols). The cumulated compressive strain evolution with depth is deduced from the official chronologies of each core.

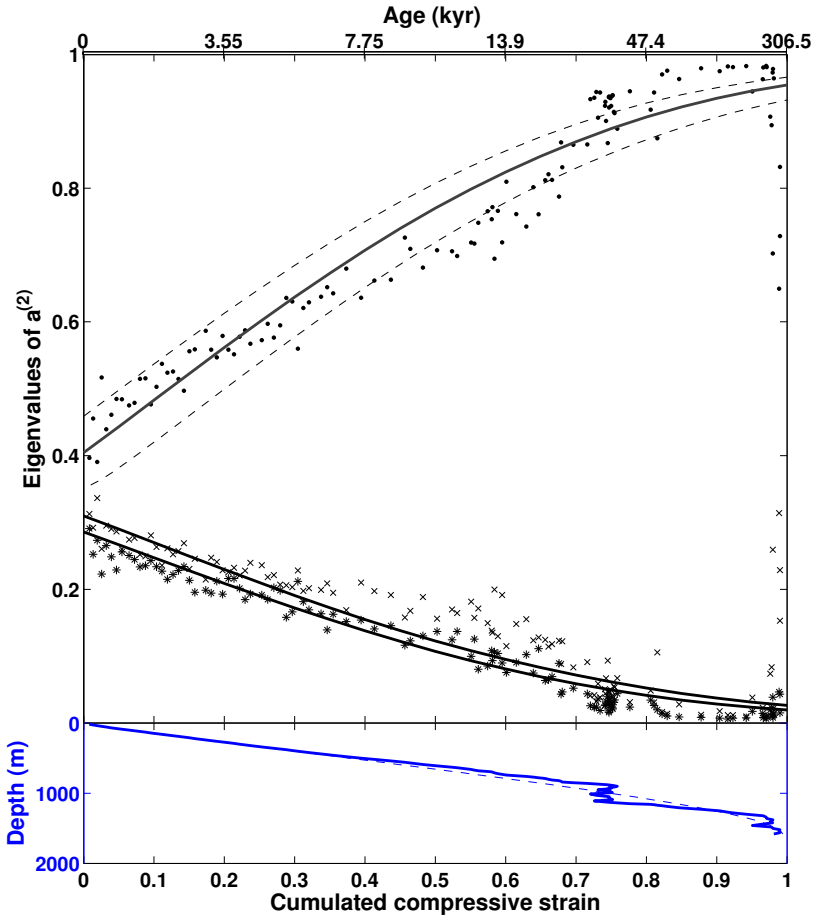

Figure 8: Upper part: evolution of $\mathbf{a}^{(2)}$ eigenvalues as a function of cumulated compressive strain. Lines = model results. Dots, crosses and plus = measurements. Dashed line represents the range of fabric evolution simulated with variations in initial eigenvalues (see text). Bottom part: evolution of the cumulated compressive strain with depth, as estimated from the thinning function extracted from TALDICE-1 chronology. Inverse model (thick line) and direct model (dashed line). Age scale is reported on the top axis.